

## Short Communication

# The Effect of Tin Weight Fraction and Annealing Condition on Electrical and Optical Properties of ITO/TiO<sub>2</sub> Nanostructured Film

Alireza Bahramian\*

Department of Chemical Engineering, Hamedan University of Technology, P.O. Box 65155, Hamedan, I. R. Iran.

(\*) Corresponding author: bahramian@hut.ac.ir  
(Received: 29 December 2016 and Accepted: 23 April 2017)

### **Abstract**

High transparent conductive indium tin oxide/titanium dioxide (ITO/TiO<sub>2</sub>) nanostructured thin film is prepared by sol-gel dip-coating technique. This method yielded monodisperse ITO nanoparticles with mean diameter of 12 nm. The atomic composition of the Sn within the ITO structure changed from 0-20 wt.%. Through controlled annealing temperature at 550 °C, the results of four-point probe technique showed that the resistivity of the ITO film depends on the Sn doping ratio, the film thickness and atmospheric conditions applied during annealing. The ITO nanostructured film with thickness of 165 nm containing 8 wt.% Sn atoms annealed under vacuum condition showed a low resistivity of  $5.1 \times 10^{-4} \Omega\text{-cm}$  and transparency as high as 90% with wavelengths between 500 and 700 nm. The refractive index and extinction coefficient of the ITO/TiO<sub>2</sub> thin film is determined by using the UV-vis spectrophotometer. An optical method is used to determine the band gap of the film. Experimental results showed that the refractive index, extinction coefficient, and band gap was closely on the atmospheric conditions and crystallinity of the ITO nanostructures. The monodispersed ITO nanostructures and its preparation methodology can be used for the fabrication of novel thin films that applied for large-scale integrated opto-electronic devices.

**Keywords:** ITO/TiO<sub>2</sub> thin film, Nanostructures, Electrical Resistance, Optical Transmittance.

## 1. INTRODUCTION

Transparent conducting oxides (TCOs) are special semiconductors that are optically transparent and electrically conductive. Among many TCO films, Indium tin oxide (ITO) as known as an n-type semiconductor, which show good conductivity and high transmission in the visible light and near-IR region [1-4]. Its transparency to visible light is related to the large band gap energy of ITO (3.4 and 4.3 eV), while its conductivity comes from its intrinsic oxygen vacancy defects and extrinsic defects caused by Sn<sup>4+</sup> doping. Nanostructured ITO Thin films are widely used in a variety of optoelectronic device applications such as electroluminescence displays, solar cells, gas sensors, flat panel

displays, liquid crystal displays and organic light emitting diodes [5-12].

Several methods such as sputtering, reactive thermal deposition, chemical vapor deposition, electron beam evaporation, spray pyrolysis and sol-gel dip-coating were reported for preparing ITO nanostructured thin films [13-18]. In the most cases, high temperature techniques are required to preparation of thin films. The sol-gel dip coating method posses several advantages like lower processing temperature, higher control on size of nanoparticles and better homogeneity of thin films [19-20].

The experimental results have shown that the preparation of high transparent thin

films by dip-coating method needs to control morphology and thickness of the film [21]. The resistivity of the ITO thin films depends on oxygen vacancies and substitution of the Sn atoms. ITO is a non-stoichiometric compound on oxygen atoms that lead to the formula  $\text{In}_{2-x}\text{Sn}_x\text{O}_{3-y}$ . The value of  $y$  depends on the Sn doping, annealing temperature and atmospheric condition of furnace during annealing process [22-23]. Doping  $\text{Sn}^{4+}$  ions leads to decreasing the  $y$  value because of incorporation of compensating oxygen atoms [24-25].

In recent years, multi-layer oxide films, such as  $\text{TiO}_2/\text{SiO}_2$  and  $\text{ITO}/\text{TiO}_2$ , provide a high visible light transmittance and good reflectance. For example, Ray et al., fabricated a multi-layer  $\text{ITO}/\text{TiO}_2$  film with more than 85% transmittance in the wavelengths above 900 nm [26]. Sawada and Taga [6] have developed an improved transparent IR reflector using a  $\text{TiO}_2/\text{ITO}$  thin film. They have succeeded in obtaining about 80% transmittance between wavelengths of 800 and 1200 nm.

In the present work, ITO nanostructured film was deposited by sol-gel dip-coating method on  $\text{TiO}_2$  thin film to develop  $\text{ITO}/\text{TiO}_2$  thin film with appropriate physical properties. The proposed method yielded monodisperse ITO nanoparticles with mean diameter of 12 nm. The resistivity of ITO films with different composition of the Sn atoms (0-20 wt. %) is analyzed. The effect of film thickness on resistivity and transparency of thin films is studied under a controlled thermal annealing condition. The optical parameters, structural properties, morphology and resistivity of the fabricated  $\text{ITO}/\text{TiO}_2$  nanostructured thin films were investigated by UV-Vis spectrophotometer, XRD, SEM, and Four-point probe technique, respectively.

## 2. MATERIAL AND METHODS

### 2.1. Synthesis of $\text{TiO}_2$ and ITO Nanostructures

The sol-gel dip-coating technique can benefit of a colloidal inorganic precursor using metal salts and alkoxides [19]. Details of the solution preparation and dip-coating of  $\text{TiO}_2$  thin film can be found in our last papers [27-28]. The ITO solution was prepared by dissolving 0.2376 g of indium nitrate trihydrate ( $\text{In}(\text{NO}_3)_3 \cdot \text{H}_2\text{O}$ , Merck, 99.9%) in 7 ml of acetylacetone (Merck,  $\geq 99.5\%$ ) under reflux at 65 °C for 30 min. A solution of ethanol (Merck,  $\geq 99.8\%$ ) and tin tetrachloride ( $\text{SnCl}_4$ , Merck,  $\geq 99.8\%$ ) is prepared by dissolving 0.0464 g of  $\text{SnCl}_4$  salt in 7 ml of ethanol at room temperature. The obtained mixture was added drop wise to the first solution under stirring. Indium ions ( $\text{In}^{3+}$ ) reacts with acetylacetone to form a chelate structure of indium - acetylacetone ( $\text{In}(\text{CH}_3\text{COCHCOCH}_3)^{2+}$ ). The obtained chelate complex expected to play a similar role to the alkoxide, where the metal ions are surrounded by oxygen atoms. Finally, the indium-acetylacetone changes to form indium (III) acetylacetonate salt ( $\text{In}(\text{CH}_3\text{COCHCOCH}_3)_3$ ).

### 2.2. Fabrication of ITO and $\text{TiO}_2$ Thin Films

Dip-coating process of  $\text{TiO}_2$  thin film as substrates in the ITO solution was performed with withdrawal velocity of  $8.3 \times 10^{-4} \text{ m.s}^{-1}$  at room temperature. The prepared films were heated at the temperature of 125 °C in an electric oven and cooled down to room temperature. The same process was repeated four times. The prepared film annealed at 550 °C in air (oxygen) and in vacuum (argon) under a heating rate of  $3 \text{ }^\circ\text{C min}^{-1}$ . The samples allowed to cool at room temperature and prepared for further analysis.

### 2.3. Characterization of the ITO and $\text{TiO}_2$ Thin Film

The structure and morphology of the  $\text{ITO}/\text{TiO}_2$  thin film is examined by scanning electron microscopy (SEM, Cam Scan MV2300 microscope). The surface morphology and roughness of the ITO

nanostructured thin films are studied by an atomic force microscope (AFM, DME DS-95-50). The film thickness was measured using a ZeScope optical profilometer.

The crystalline phase of TiO<sub>2</sub> and ITO nanostructures were determined by X-ray diffraction method (XRD, Philips PW 1800 diffractometer with Cu K $\alpha$  radiation). Transmittance of the film is measured by a UV-Vis spectrophotometer (Hitachi U-3140) in the range of 300-1000 nm. The resistivity of the films is measured using the four-point probe method.

### 3. RESULTS AND DISCUSSION

#### 3.1 Crystallinity of the ITO and TiO<sub>2</sub>

Figure 1 shows the XRD patterns of nanostructured ITO film (Fig. 1a-b) and TiO<sub>2</sub> thin film (Fig. 1c) annealed at 550 °C in air (Fig. 1a) and in vacuum (Fig. 1b). A maximum peak intensity corresponding to the (222) predominant orientation can be seen at 30° (Fig. 1 a-b). Other peaks are (211), (400), (332), (431), (440) and (622) planes, which exhibits a bixbyite structure of ITO with a unit cell containing 40 atoms and two non-equivalent cation sites [1-3]. The intensity of each peak was measured through fitting and integrating of the Gaussian function. The peaks suggested that the film annealed in the vacuum has high portion of (400)-oriented peak in compared to the annealed film in the air. The  $I_{(222)}/I_{(222)+I_{(400)}}$  peak ratio, which is represent in XRD pattern of the film annealed in air condition, is high in comparison with the film that annealed under vacuum condition.

During heat treatment, oxygen atoms would be absorbed on the substrate or the film surface. Therefore, the In and Sn atoms are easily trapped by the oxygen atoms. The average mobility of In and Sn atoms is decrease in the air conditions that lead to increase in (222)-peak intensity. The peak ratio of the (400/222) was ~0.4, yielding low sheet resistance in the ITO films [29, 30]. Figure 1c shows a pronounced (101) peak of TiO<sub>2</sub> at 25°,

suggesting that the anatase phase. Other peaks are observed at (004), (211), and (116) planes. None of the spectra showed any characteristic peaks of Sn, SnO and SnO<sub>2</sub>, which means that the Sn atoms were doped substitutionally in the In<sub>2</sub>O<sub>3</sub> crystal lattice. The average crystalline size of ITO particles is determined by the (222) peak broadening by Scherrer's equation. The mean size of the ITO particles annealed in vacuum and in air is found to be 18 and 24 nm, respectively. This result means the crystallite size of the ITO nanoparticles depends on the applied annealing atmosphere.

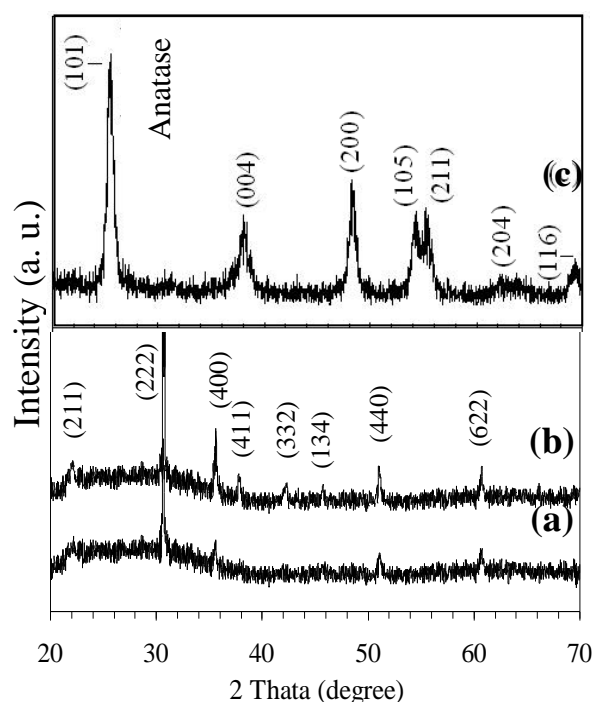


**Figure 1.** The XRD patterns of ITO (a, b) and TiO<sub>2</sub> (c) thin film annealed at 550 °C in air (a) and in vacuum (b).

#### 3.2. Structural Properties of the ITO and TiO<sub>2</sub> Thin Film

Figure 2 shows the SEM image of TiO<sub>2</sub> (Fig. 2a and 2c) and ITO nanostructured film (Fig. 2b and 2d). Figures 2a and 2b show low-magnification SEM image of TiO<sub>2</sub> and ITO thin film, respectively. It can be seen that the TiO<sub>2</sub> nanorods are formed on the film surface (Fig. 2a), which may

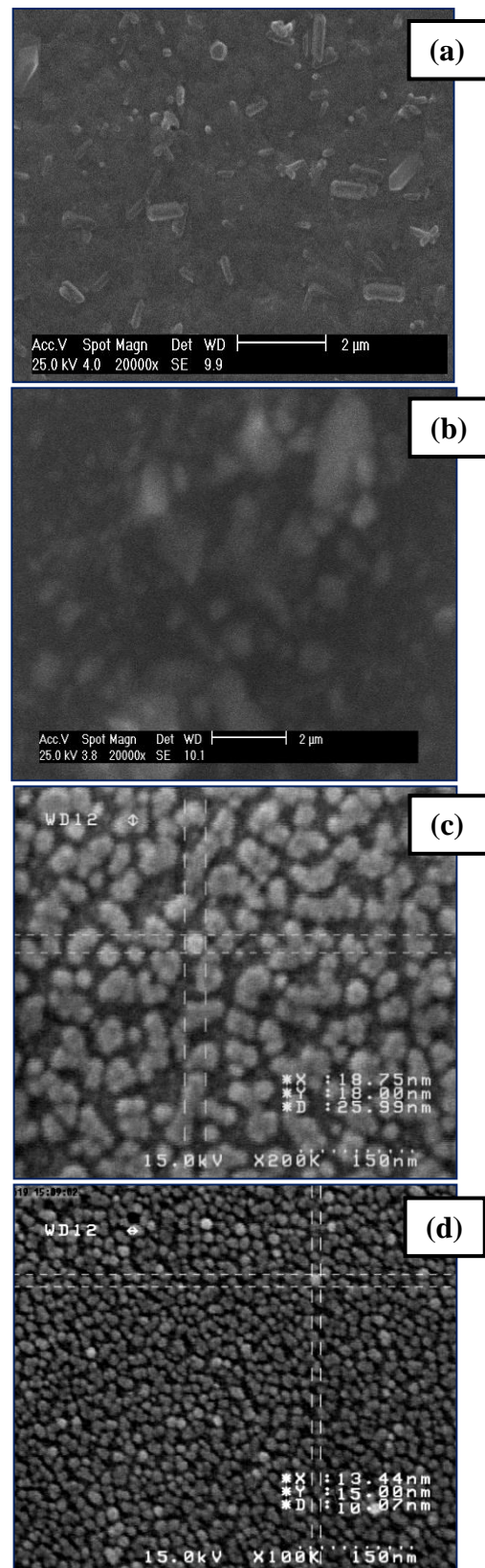
undergo a crystal growth of the TiO<sub>2</sub> nanoparticles as governed by the surface charges and surface energy.

Figure 2b shows the large quantities of the ITO nanoparticles with tip edges were formed on the film surface. Figures 2c and 2d show the high-magnification SEM image of TiO<sub>2</sub> and ITO thin film, respectively. Figure 2c shows a fairly uniform distribution of nanoparticles on the film surface. Also, the ITO nanostructured film had more homogenously distributed particle size and more uniform shapes than TiO<sub>2</sub> thin film. Detailed SEM analysis on the ITO film that annealed in vacuum showed no evidence aggregation/sintering or cracks on the film surface. Figure 2d shows the uniform surface of ITO nanostructured film with mean particle diameter of 12 nm. Typically, the size of particles is between 10.07-15.00 nm.

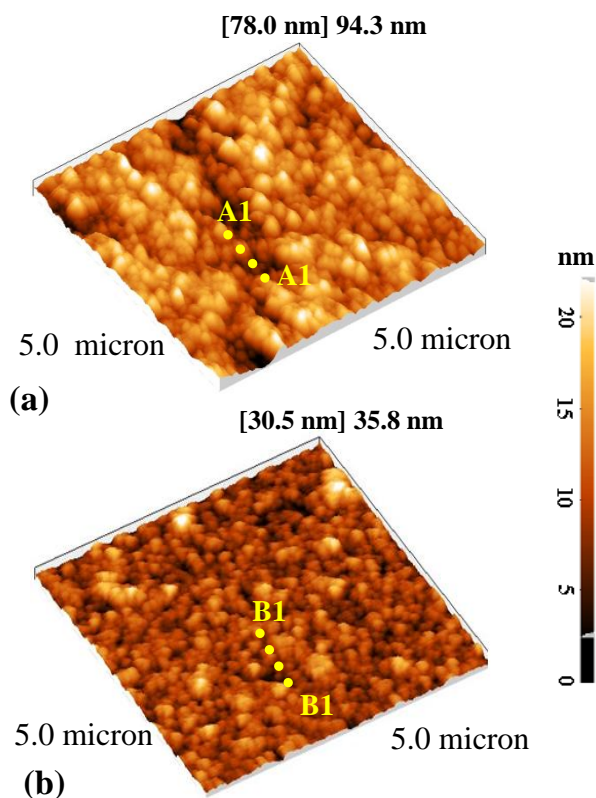
Figure 3 shows the AFM image of TiO<sub>2</sub> (Fig. 3a) and ITO film (Fig. 3b). It can be seen that the TiO<sub>2</sub> surface shows a rough surface with trenches compared with the ITO nanostructured film. AFM images show that the particle size in ITO nanostructured films is smaller compared with the TiO<sub>2</sub> film; which result the ITO nanostructured films possess larger surface area. AFM images analysis showed that the ITO nanostructured film has a smooth surface over a 25 μm<sup>2</sup> with a root-mean-square surface roughness of 4.56 nm.

Figure 4 illustrates the variation in the height of the summits as determined by the AFM analysis for the prepared TiO<sub>2</sub> (Fig. 4a) and ITO (Fig. 4b) film. Images are lines profile along the A1–A1 and B1–B1 in Fig. 3, respectively.

The AFM analysis shows that the surface morphology of TiO<sub>2</sub> film show fairly uniform morphology, while ITO nanostructured film shows homogenous structure of smooth surface. The total thickness of ITO/TiO<sub>2</sub> film was determined by ZeScope optical profilometer to be 405±5 nm.



**Figure 2.** SEM images of (a) TiO<sub>2</sub> thin film and (b) ITO nanostructured film. [(a-b) are low-magnification and (c-d) are high-magnification images, respectively].



**Figure 3.** AFM images of (a)  $\text{TiO}_2$  thin film and (b) ITO nanostructured film.

### 3.3. Electrical Properties of ITO Film

The sheet resistivity of ITO nanostructured films is studied to achieve efficient charge transport of the metal oxide through controlled Sn-doping. Figure 5 shows the Sn-weight ratio dependent resistivity of the ITO film annealed at  $550^\circ\text{C}$  in the vacuum and in air. The annealing temperature is selected based on the literature [21, 23]. Alam and Cameron reported a large reduction in resistivity of the ITO film, when the temperature was up to  $500^\circ\text{C}$  [32].

According to Figure 5, it can be seen that when  $\text{Sn}^{4+}$  is doped into  $\text{In}_2\text{O}_3$  in low values (0-8 wt.%), the resistivity of the ITO film decreases sharply with increasing  $\text{Sn}^{4+}$  doping level, but beyond 8 wt.% Sn atomic ratio showed a resistivity of  $5.1 \times 10^{-4} \Omega\text{-cm}$ , the resistivity increases when Sn atomic ratio increases from 8 to 20 wt.%. This resistivity trend is consistent with previous studies [24].

The sheet resistances of the ITO films annealed in air were higher than that heat-treated in vacuum.

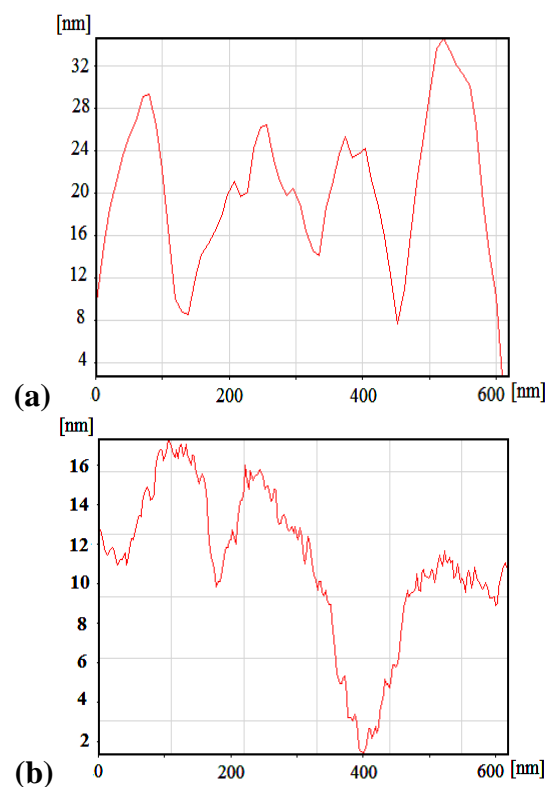
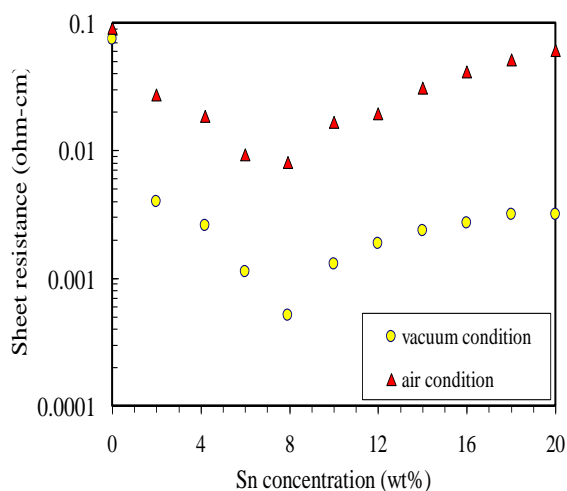


**Figure 4.** AFM image analysis of (a)  $\text{TiO}_2$  and (b) ITO nanostructured film. [a and b images are lines profile along the A1–A1 and B1–B1 in Fig. 3, respectively].

The difference observed in resistivity between the two atmospheric conditions is explained by the difference in Sn concentration and oxygen vacancy sites in the ITO crystal lattice [24, 25]. At first, the sheet resistivity of the ITO films annealed in the air does not increase considerably with increases in Sn-doping, which is believed to have low electron mobility. Second, the oxygen vacancy sites stands between the valence and the conduction bands, which are responsible for the lower resistivity of the ITO films.

The oxygen atoms existing freely on the ITO structure heated in the air because of developing a fine crystallite structure in compared with the vacuum. Fallah et al. showed that not all of the Sn atoms can be substituted into indium atom sites with increasing Sn doping, in other word, all of tin atoms do not behave as effective donors. Therefore, low values of  $\text{Sn}^{4+}$  ions are transformed into  $\text{Sn}^{2+}$ , which acts as acceptors [21]. Chan et al. reported that the

oxygen partial pressure has a strong effect on the sheet resistances of ITO nanostructured films [33]. They found that the decrease in sheet resistance due to increasing oxygen partial pressure is attributed to enhanced electron mobility in stoichiometric ITO thin film.



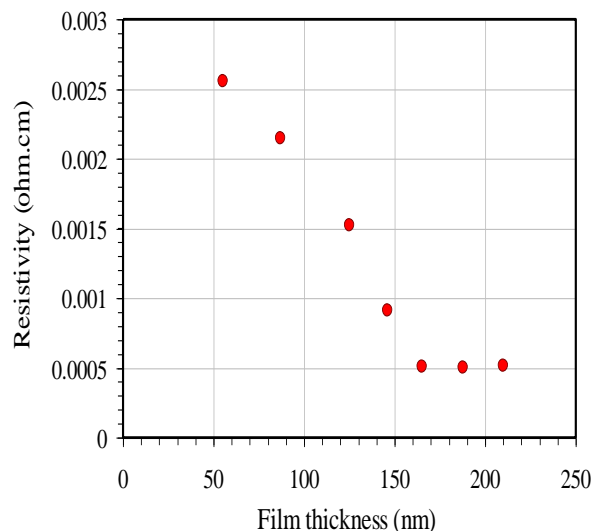
**Figure 5.** Sheet resistance of the ITO nanostructured film as a function of Sn doping at annealing atmosphere of (a) air, and (b) vacuum.

Figure 6 shows the thickness-dependent resistivity of the ITO nanostructured film annealed at 550 °C in the vacuum. For ITO nanostructures with Sn composition fixed at 8 wt.%, the resistivity decreases up to thickness values of 140 nm and then remain relatively constant. As a result, The 165 nm thick ITO nanostructured film containing 8 wt.% Sn atoms annealed at 550 °C under vacuum condition showed a resistivity of  $5.1 \times 10^{-4} \Omega\text{-cm}$ .

### 3.4. Optical Properties of ITO Film

Figure 7 shows the transmittance spectrum of ITO and TiO<sub>2</sub> thin films annealed at 550 °C on glass slide between the wavelength of 300 and 1000 nm.

The thickness of ITO and TiO<sub>2</sub> films are determined  $165 \pm 8$  nm and  $240 \pm 10$  nm, respectively. The thickness of glass slides were 2 mm. All thin films annealed at 550 °C in the vacuum and in air.



**Figure 6.** Resistivity changes as a function of the ITO film thickness containing 8 wt.% Sn annealed at 550 °C in the vacuum.

The typical maximum ( $T_M$ ) and minimum ( $T_m$ ) of the oscillating transmittance of the ITO nanostructured film annealed at 550 °C in the air is shown in Fig. 7b.

It can be seen from Fig. 7a that the transmittance of films is about 90% in the wavelengths between 500 and 700 nm. A small difference exists in the transmittance levels between the prepared films annealed in the air and vacuum condition. Each of the spectra can be divided into two regions: a transparent raising region and a zone of strong and stable transmittance. The fast decrease below about 380 nm is caused by light absorption under excitation of electrons from the valence band to the conduction band of metal oxides.

The curves with stable and strong transmittance between 380 and 800 nm are caused by the interference between the film and the glass substrate. Details of the optical properties of nanostructured TiO<sub>2</sub> thin film on the glass slide can be found in our last paper [28].

The optical constants such as the refractive index  $n(\lambda)$  and the extinction coefficient  $k(\lambda)$  of the ITO/TiO<sub>2</sub> film were calculated from the transmittance spectrum

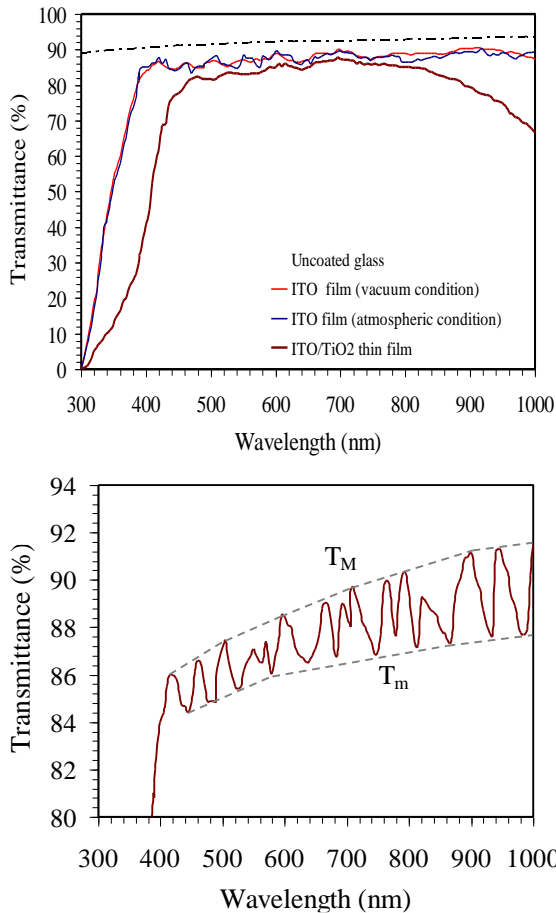


**Figure 7.** (a) Transmittance spectra of ITO and TiO<sub>2</sub> films annealed at 550 °C, (b) Typical maximum and minimum of the oscillating transmittance of the ITO film.

following the method proposed by Manificier and Swanepoel [34, 35].

If two envelopes are drawn through the maximum  $T_M(\lambda)$  and minimum  $T_m(\lambda)$  of the oscillating transmittance, the refractive index will be given as:

$$n(\lambda) = \sqrt{N(\lambda) + \sqrt{N^2(\lambda) - s^2(\lambda)}} \quad (1)$$

where

$$N(\lambda) = 2s(\lambda) \frac{T_M(\lambda) - T_m(\lambda)}{T_M(\lambda) \times T_m(\lambda)} + \frac{s^2(\lambda) + 1}{2} \quad (2)$$

here  $T_M$  and  $T_m$  can be calculated in term of

$$T_M(\lambda) = \frac{1}{\frac{1}{T_m(\lambda)} - A(\lambda)} \quad (3)$$

$$T_m(\lambda) = \frac{1}{\frac{1}{T_M(\lambda)} + A(\lambda)} \quad (4)$$

and

$$A(\lambda) = \frac{m^4 \lambda^4 + 16 s(\lambda)^2 d^4 - 4 d^2 m^2 \lambda^2 (1 + s(\lambda)^2)}{16 s(\lambda) d^2 m^2 \lambda^2} \quad (5)$$

$s(\lambda)$  is the refractive index of glass slide. Considering the glass substrate alone in the absence of a film,  $s(\lambda)$  is given by:

$$s(\lambda) = \frac{1}{T_s(\lambda)} + \sqrt{\left(\frac{1}{T_s(\lambda)} - 1\right)} \quad (6)$$

where  $T_s(\lambda)$  is the transmission of the glass slide in the absence of metal oxide film.

The basic equation for interference fringes is given by:

$$2 n(\lambda) d = m \lambda \quad (7)$$

here  $m$  is an integer for peak values and half integer for valleys. If  $d$  is measured, the refractive index of peaks and valleys can be calculated by equation 1.

Based on the Manificier and Swanepoel's method, the values of the  $T_M$  and  $T_m$  were estimated by measuring the real thickness of the thin film [34, 35]. But, it was found that the calculated  $T_M$  derived from the real thickness of the thin film was larger than 100% ( $T_M = 107.2\%$ ,  $T_m = 104.5\%$ ). It is obvious that the calculated  $n(\lambda)$  obtained by fitting the curves of  $T_M$  and  $T_m$ , (Fig. 7b), slightly deviates from the real value of the refractive index. One of the main reason for this deviation is that in equation 1,  $k(\lambda)$  is considered to be zero, while the value of  $k(\lambda)$  is not equal to zero and the transmission is sensitive to this parameter [17, 26, 35]. Therefore, equation 2 can only give an approximate value of  $n(\lambda)$ . The value of  $k(\lambda)$  can be calculated from the following equation [26]:

$$k(\lambda) = \alpha(\lambda) / 4 \quad (8)$$

where  $\alpha(\lambda)$  is the absorption coefficient given by

$$\alpha(\lambda) = -\frac{\ln x(\lambda)}{d} \quad (9)$$

here  $x(\lambda)$  is the absorbance and is given as

$$x(\lambda) = \frac{E_M \left\{ E_M^2(\lambda) - [n^2(\lambda) - 1]^3 [n^2(\lambda) - s^4(\lambda)] \right\}^{1/2}}{[n^2(\lambda) - 1]^3 [n(\lambda) - s^2(\lambda)]} \quad (10)$$

and

$$E_M = \frac{8n^2(\lambda)s(\lambda)}{T_M(\lambda)} + \left[ n^2(\lambda) - 1 \right] \left[ n^2(\lambda) - s^2(\lambda) \right] \quad (11)$$

Substituting  $\alpha(\lambda)$  into equation 8 results the  $k(\lambda)$  value.

Figure 8 shows the calculated values of refractive index (Fig. 8a) and extinction coefficient (Fig. 8b) of ITO and ITO/TiO<sub>2</sub> film as a function of the wavelength. The ITO film was transparent at wavelengths greater than 430 nm as the reflection of the incident light was effectively suppressed. The refractive index at a wavelength of 430 nm is found to be about 1.834 (Fig. 8a), which is lower than that of polycrystalline ITO thin films reported by other researchers ( $n = 1.91$  [17], 2.01 [24] and 1.96 [26]).

According to Fig. 8a, it can be seen that the ITO film annealed under vacuum shows a lower refractive index in comparison with the ITO film annealed in the atmospheric condition. It can be explained by more (400) oriented crystal structure that have been resulted in lower refractive index. In most cases, ITO films crystallize in cubic bixbyite structures are optically isotropic. Therefore, the perpendicular crystallographic planes in ITO films have an optical symmetry with each other. But, (222) and (400) peaks, which are the main crystallographic orientations of the ITO thin films fabricated in this work are not perpendicular. The ITO films with a perfect (222) or a (400) oriented peak have various optical constants in the perpendicular direction to substrates because of unlike energy of electrons and different atomic arrangements.

Figure 8b shows the calculated  $k(\lambda)$  of ITO/TiO<sub>2</sub> and ITO nanostructured films in the vacuum and in air. The values of  $k(\lambda)$  obtained for ITO/TiO<sub>2</sub> film heated under vacuum and air were found to be about  $6.2 \times 10^{-3}$  and  $5.1 \times 10^{-3}$  respectively. Nevertheless, these values are lower than that of ITO thin films ( $7.43 \times 10^{-3}$ ) [35].

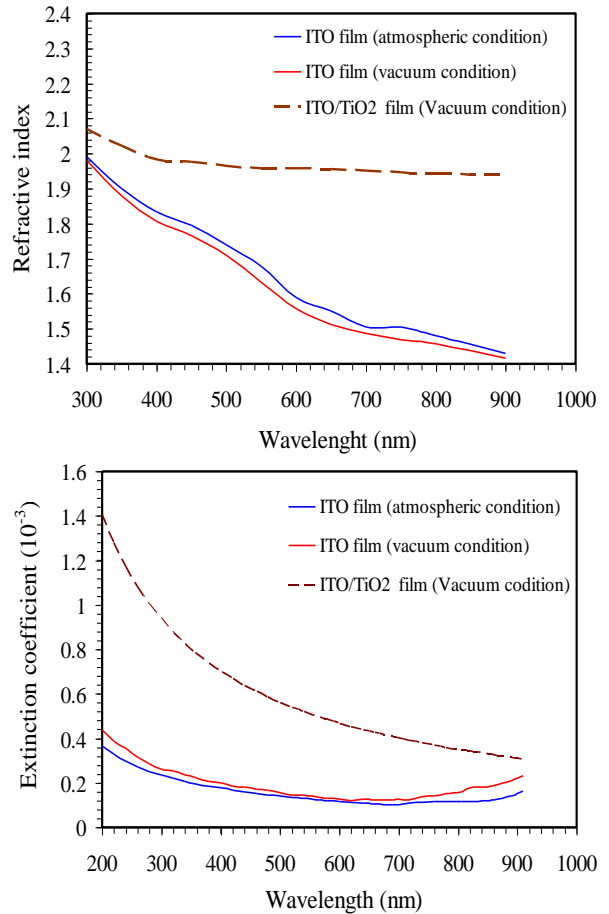


**Figure 8.** Refractive index (a) and extinction coefficient (b) of ITO (solid line) and ITO/TiO<sub>2</sub> films (dashed line)

As shown in figure 8b, higher free carrier density seems to be responsible for higher extinction coefficients in the near infrared region, which indicates good crystallinity of the ITO film heated under vacuum. The changes in extinction coefficients are different between the visible range ( $\approx 400$ -700 nm) and the near infrared region ( $> 700$  nm). In the visible range, the extinction coefficients of samples are close together, while in the near infrared region, atmospheric conditions applied during annealing process lead to difference in the extinction coefficients of ITO films [36, 37].

It is worthy of attention to interpret the complex refractive index  $R$  of an ITO/TiO<sub>2</sub> thin film, which is given by: [26, 38]

$$R = \left( 1 - \frac{n_2}{n_1} \right)^2 / \left( 1 + \frac{n_2}{n_1} \right)^2 \quad (12)$$

The complex refractive index gives the fraction of reflected light at the interface of ITO/TiO<sub>2</sub> film. Here  $n_1$  and  $n_2$  are the real parts of the complex refractive indexes of TiO<sub>2</sub> and ITO, respectively. The optical band gap ( $E_g$ ) of the ITO and TiO<sub>2</sub> films were estimated by assuming a direct transition between valence and conduction bands. Figure 9 shows the plotting  $[\alpha(\lambda)hv]^2$  relative to photon energy ( $hv$ ) of ITO/TiO<sub>2</sub> thin film [35].

A linear relation exists in a certain range, thus supporting the assumption of a direct transition. The  $E_g$  of the ITO/TiO<sub>2</sub> thin film can be calculated by extrapolating the linear portion of a plot of  $[\alpha(\lambda)hv]^2$  versus ( $hv$ ) to  $[\alpha(\lambda)hv]^2 = 0$ . According to this method, the  $E_g$  of the ITO/TiO<sub>2</sub> thin film annealed in the air and in vacuum are about 3.77 and 3.86 eV, respectively, which are higher than that of ITO thin film (3.67 eV) [38-40]. It appears that the difference is mainly due to quantum size effect and existence of amorphous phase in the ITO/TiO<sub>2</sub> thin film. The quantum-size effect resulted in a dramatic increase in the band gap energy if the crystallite dimensions became very small.

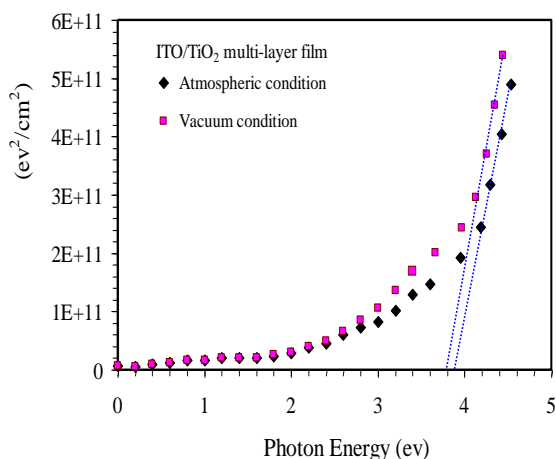


**Figure 9.** Plot of  $(\alpha hv)^2$  versus photon energy (eV) of ITO/TiO<sub>2</sub> thin film annealed at different conditions. The band gap energy is deduced from extrapolation of the straight line to  $[\alpha(\lambda)hv]^2 = 0$ .

### 3- CONCLUSION

High transparent conductive ITO/TiO<sub>2</sub> nanostructured thin film is prepared by a

sol-gel dip-coating method. The ITO nanoparticles with mean diameter of 12 nm and a root-mean-square roughness of 4.56 nm are deposited uniformly on the TiO<sub>2</sub> thin film. This method yielded ITO nanostructured film with Sn concentration between 0-20 wt.%. Through controlled annealing temperature at 550°C, the results of four-point probe technique showed that the resistivity of the nanocrystalline ITO film depends on the Sn doping, the thickness of the prepared film and atmospheric conditions applied during annealing. The experimental results showed that the annealing under vacuum condition leads to the reduction of the sheet resistance of the ITO film. The 165 nm thick ITO nanostructured film containing 8 wt.% Sn atoms annealed under vacuum condition showed a low resistivity of  $5.1 \times 10^{-4} \Omega\text{-cm}$  and transparency as high as 90% in the visible light.

The experimental results showed that the refractive index, extinction coefficient, and band gap are closely related to the atmospheric conditions and crystallinity of the ITO nanostructures. The calculated value of refractive index obtained from the transmittance spectrum showed that the ITO film annealed in the vacuum has a lower value in comparison with the film annealed in the air. It can be explained by more (400) oriented structure that resulted in lower refractive index. Thus, the films with higher refractive index had more (222)-oriented crystallographic structures. The complex refractive index of the ITO/TiO<sub>2</sub> film is also calculated from the individual refractive index of ITO and TiO<sub>2</sub> thin films. The extinction coefficient obtained for ITO/TiO<sub>2</sub> thin film heated in the air and in the vacuum are found to be about  $6.2 \times 10^{-3}$  and  $5.1 \times 10^{-3}$ , respectively. The optical method showed that the band gap of the ITO/TiO<sub>2</sub> thin film annealed in the air and in the vacuum are 3.77 and 3.86 eV, respectively. This novel monodisperse ITO structure and its fabrication

methodology can be used in large-scale producing of *n*-type semiconductors.

## REFERENCES

1. Yun, J., Park, Y. H., Bae, T. S., Lee, S., Lee, G. H. (2013). "Fabrication of a Completely Transparent and Highly Flexible ITO Nanoparticle Electrode at Room Temperature", *ACS Appl. Mater. Interfaces*, 5: 164-172.
2. Thirumoorthi, M., Joseph Prakash, J. T. (2016). "Structure, Optical and Electrical Properties of Indium Tin Oxide Ultra Thin Films prepared by Jet Nebulizer Spray Pyrolysis Technique", *J. Asian Ceram. Soc.*, 4: 124-132.
3. Brewer, S. H., Franzen. S. (2004). "Calculation of the Electronic and Optical Properties of Indium Tin Oxide by Density Functional Theory", *Chem. Phys.*, 300: 285-293.
4. Singh, P., Kumar, A., Kaur. D., (2008). "Growth and Characterization of New Nonlinear Optical Thiourea-alanine Acetate Single Crystal", *J. Phys. B.*, 403: 3769-3773.
5. Kesim, M. T., Durucan. C. (2013). "Indium Tin Oxide Thin Films Elaborated by Sol-gel Routes: The Effect of Oxalic Acid Addition on Optoelectronic Properties", *Thin Solid Films*, 545: 56-63.
6. Chopra, K. L., Major, S., Pandya. D. K. (1983). "Thin-Film Solar Cells: An Overview", *Thin Solid Films*, 108: 333-340.
7. Schropp, R. E. I., Li, H., Rath, J. K., van der Werf. C. H. M. (2008). "Growth Mechanism of Nanocrystalline Silicon at the Phase Transition and Its Application in Thin Film Solar Cells", *Surf. Interface Anal.*, 40: 970-973.
8. Xia N., Gerhardt, R. A. (2016). "Fabrication and Characterization of Highly Transparent and Conductive Indium tin Oxide Films made with Different Solution-based Methods", *Mat. Res. Express*, 4: 116408-116414.
9. Fortunato, E., Barquinha, P., Martins, R. (2012). "Oxide Semiconductor Thin-Film Transistors: A Review of Recent Advances", *Adv. Mat.* 24: 2945-2986.
10. Cindemir, U., Lansåker, P., Österlund, L., Niklasson, G. A., Granqvist, C. G. (2016). "Sputter-Deposited Indium-Tin Oxide Thin Films for Acetaldehyde Gas Sensing", *Coatings*, 6: 19-26.
11. Yadav, B. C., Agrahari, K., Singh, S., Yadav, T. P. (2016). "Fabrication and Characterization of Nanostructured Indium Tin Oxide film and Its Application as Humidity and Gas Sensors", *J. Materials Sci: Materials in Electronics*, 27: 4172-4179.
12. Ok, K. H., Kim, J., Park, S. R., Kim, Y., Lee, C. J., Hong, S. J., Kwak, M. G., Kim, N., Han, C. J., Kim, J. W. (2015). "Ultra-thin and Smooth Transparent Electrode for Flexible and Leakage-free Organic Light-emitting Diodes", *Sci. Rep.*, 5: 1-8.
13. Habibi; M. H. Khaledi Sardashti, M. (2008). "Preparation and Proposed Mechanism of ZnO Nanostructure Thin Film on Glass with Highest *c*-axis Orientation", *Int. J. Nanosci. Nanotechnol.*, 4: 13-16.
14. Kamei, M., Shigesato, Y., Takaki. S. (1995). "Origin of Characteristic Grain-subgrain Structure of Tin-doped Indium Oxide Films", *Thin Solid Films*, 259: 38-45.
15. Hartmann, P., Lee, D. K., Smarsly, B., Janek. M. (2010). "Mesoporous TiO<sub>2</sub>: Comparison of Classical Sol-Gel and Nanoparticle Based Photoelectrodes for the Water Splitting Reaction", *ACS Nano*, 4: 3147-3154.
16. Elmas, S., Korkmaz, S., Pat. S., (2013). "Optical Characterization of Deposited ITO Thin Films on Glass and PET Substrates", *Appl. Surf. Sci.*, 276: 641-645.
17. Lakshmi, J. S., John Berlin, I., Daniel, G. P., Thomas, P. V., Joy, K. (2011). "Effect of Calcination Atmosphere on Photoluminescence Properties of Nanocrystalline ZrO<sub>2</sub> Thin Films Prepared by Sol-gel Dip Coating Method", *J. Phys. Condens. Matter*, 406: 3050-3055.
18. Golobostanfard, M. R., Abdizadeh, H. (2013). "Effects of Acid Catalyst Type on structural, Morphological, and Optoelectrical Properties of Spin-coated TiO<sub>2</sub> Thin", *J. Phys. Condens. Matter*, 413: 40-46.
19. Ramanan, S. R. (2001). "Dip Coated ITO Thin-Films Through Sol-gel Process Using Metal Salts", *Thin Solid Films*, 389: 207-212.
20. Fallah, H. R., Ghasemi, M., Hassanzadeh, A., Steki, H. (2006). The Effect of Deposition rate on Electrical, Optical and Structural Properties of Tin-doped Indium Oxide (ITO) Films on Glass at Low Substrate Temperature", *J. Phys. B.*, 373: 274-279.
21. Bahramian, A. (2013). "High Conversion Efficiency of Dye-Sensitized Solar Cells Based on Coral-like TiO<sub>2</sub> Nanostructured Films: Synthesis and Physical Characterization", *Ind. Eng. Chem. Res.* 52: 14837-14846.
22. Falahatgar, S. S., Ghodsi F. E. (2016). "Annealing Temperature Effects on the Optical Properties of MnO<sub>2</sub>: Cu Nanostructured Thin Films", *Int. J. Nonosci. Nanotechnol.*, 12: 7-18.
23. Lee, J., Lee, S., Li, G., Petruska, M. A., Paine, D. C., Sun, S. (2012). "A Facile Solution-Phase Approach to Transparent and Conducting ITO Nanocrystal Assemblies", *J. Am. Chem. Soc.*, 134: 13410-13414.

24. Gaarenstroom, S. W., Balogh, M. P Militello, M. C., Waldo, R. A., Wong, C. A., Kelly, N. A., Gibson, T. L., Kundrat, M. D., (2005). "Characterization of Indium-tin-oxide Films with Improved Corrosion Resistance", *Surf. Interface Anal.*, 37: 385-392.
25. Islam M. A., Rahman K. S., Haque F., Khan N. A., Akhtaruzzaman M., Alam M. M., Ruslan H., Sopian K., Amin, N. (2015). "Effect of Sn Doping on the Properties of Nano-Structured ZnO Thin Films Deposited by Co-Sputtering Technique", *Int. J. Nanosci Nanotechnol.*, 15: 9184-9191.
26. Das, R., Ray, S. (2003). "Zinc oxide-a Transparent, Conducting IR-reflector Prepared by RF-magnetron Sputtering." *J. Phys. D: Appl. Phys.*, 36: 152-159.
27. Sasani Ghamsari, M., Bahramian, A. (2008). "High Transparent Sol-gel Derived Nanostructured TiO<sub>2</sub> Thin Film", *Mat. Let.*, 62: 361-364.
28. Bahramian, A. (2013). "Study on Growth Rate of TiO<sub>2</sub> Nanostructured Thin Films: Simulation by Molecular Dynamics Approach and Modeling by Artificial Neural Network", *Surf. Interface Anal.*, 45: 1727-1736.
29. Tao, P., Viswanath, A., Schadler, L. S., Benicewicz, B. C., Siegel, R. W., (2011). "Preparation and Optical Properties of Indium Tin Oxide/Epoxy Nanocomposites with Polyglycidyl Methacrylate Grafted Nanoparticles", *ACS Appl. Mater. Interfaces*, 3: 3638-3645.
30. Hong, S. J., Han, J. I. (2006). "Indium Tin Oxide Thin Film Fabricated by Indium-Tin-Organic Sol including ITO Nanoparticle", *Curr. Appl. Phys.*, 6: 206-210.
31. Cullity, B. D. (1978) "*Elements of X-ray Diffraction*", 2<sup>nd</sup> ed., Addison-Wesley, California.
32. Alam, M. J., Cameron, D. C. (2001). "Characterization of Transparent Conductive ITO Thin Films Deposited on Titanium Dioxide Film by a Sol-gel Process", *Surf. Coat. Technol.*, 142: 776-780.
33. Chan, Sh. H., Li, M. Ch., Wei, H. S., Chen, Sh. H. Kuo, Ch. Ch. (2015). "The Effect of Annealing on Nanothick Indium Tin Oxide Transparent Conductive Films for Touch Sensors", *J. Nanomaterials*, 2015: 1-5.
34. Manifacier, J. C., Gasiot, J., Fillard, J. P. (1976). "A Simple Method for the Determination of the Optical Constants n, k and the Thickness of a Weakly Absorbing Thin Film", *J. Phys. E, Sci. Instrument.*, 9: 1002-1004.
35. Swanepoel, R. (1983). "Determination of the Thickness and Optical Constants of Amorphous Silicon", *J. Phys. E, Sci. Instrument.* 16: 1214-1237. Mohamed, S.H., El-Hossary, F.M., Gamal, G.A., Kahlid, M.M. (2009). "Properties of Indium Tin Oxide Thin Films Deposited on Polymer Substrates", *Acta Physica Polonica A*, 115: 704-708.
36. Sengupta, D., Das, P., Mondal, B., Mukherjee, K. (2016). "Effects of Doping, Morphology and Film-thickness of Photo-anode Materials for dye Sensitized Solar Cell Application—A review", *Renew. Sustainable Energy Rev.*, 60: 356-376
37. Ray, S., Dutta, U., Das, R., Chatterjee, P. (2007). "Modelling of Experimentally Measured Optical Characteristics of ITO/TiO<sub>2</sub> Transparent Multi-layer Heat Shields", *J. Phys. D: Appl. Phys.* 40: 2445-2451.
38. Fotsa-Ngaffo, F., Caricato, A. P., Romano, F. (2009) "Optical Properties of ITO/TiO<sub>2</sub> Single and Double Layer Thin Films Deposited by RPLAD", *Appl. Surf. Sci.*, 255: 9684-9687.
39. Arunachalam, A., Dhanapandian, S., Manoharan, C., Sridhar, R. (2015). "Characterization of Sprayed TiO<sub>2</sub> on ITO Substrates for Solar Cell Applications", *Spectrochimica Acta Part A*, 149: 904-912.
40. Ok, J.-W., Kwak, D.-J. Kim, S.-H., Sung, Y.-M. (2014). "Conductive and Transparency Characteristics of Titanium-doped Indium-tin oxide (InSnO<sub>2</sub>:Ti) Films Deposited by Radio Frequency Magnetron Sputtering", *Vacuum*, 110: 196-201.